

Influence of Target Dynamic RCS Characteristics on Active Cancellation

Yongqiang Yang, Lifeng Wang, Guodong Zhao, *Member, IAENG*, Cheng Cheng

Abstract—This paper investigates active cancellation techniques for radar stealth applications, focusing on linear frequency modulated (LFM) and nonlinear frequency modulated (NLFM) signals using the Nth-order spectrum spread and compression (SSC) algorithm. A comprehensive analysis is presented incorporating realistic radar cross section (RCS) fluctuations through Swerling, chi-square, and mixed distribution models. The relationships between cancellation effectiveness and key parameters, including RCS calculation errors, signal delay times, and algorithm order are examined. For LFM signals, effective cancellation is achieved even with significant RCS calculation errors through appropriate parameter adjustment. Taylor window-based and tangent-based NLFM signals demonstrate robust cancellation capabilities, particularly at small delay times. The introduction of a novel mixed distribution model reveals that the proposed cancellation approach remains effective under more realistic RCS fluctuation conditions, with optimal performance achieved through slight under-cancellation. Numerical simulations validate that the proposed approach significantly reduces radar detection probability across various operational scenarios and achieves omnidirectional stealth capabilities for different aircraft configurations.

Index Terms—Radar stealth, RCS fluctuation, active cancellation, cancelling signal, detection probability.

I. INTRODUCTION

RADAR Cross Section (RCS) is a critical parameter for assessing the stealth performance of an aircraft target. Radar stealth technology, also known as low-observable technology, refers to methods that ensure a target is detected with a very low probability. Although RCS is a significant parameter of the target, it does not directly indicate the detection probability when the target is exposed to searching radar [1], [2], [3]. Radar detection fundamentally presents a probabilistic challenge, and the target's fluctuating RCS values necessitate a probabilistic description of the target's detection performance. The dynamic RCS characteristics of a target emphasize that detection occurs under realistic conditions, where the target echo is influenced by both its movement (including translational and micro-motion) and its real-time varying attitude angle relative to the incident wave [4], [5]. Therefore, constructing the target echo signal must account for the target's dynamic RCS characteristics.

Manuscript received August 26, 2024; revised February 5, 2025.

Yongqiang Yang is a researcher of Beijing Polytechnic College, China e-mail: (yangyq@yeah.net).

Lifeng Wang is an associate professor of the School of Aeronautic Science and Engineering, Beihang University, Beijing 100191 China e-mail: (wanglifeng@buaa.edu.cn).

Guodong Zhao is a PhD candidate of the School of Aeronautic Science and Engineering, Beihang University, Beijing 100191 China e-mail: (zhaoguodong00@buaa.edu.cn).

Cheng Cheng is a researcher of the Chinese People's Liberation Army Ground Force Equipment Department Aviation Military Representative Office in Jingdezhen Area, Jindezhen, 333000 China e-mail: (chengcheng@126.com).

An efficient method to acquire the target RCS fluctuation characteristics is through measurement. However, this approach is costly and cannot capture all possible target orientations. Classical statistical models are often employed to describe the target's fluctuating RCS data. Researchers have proposed various distribution models from a statistical perspective [6], [7], [8]. These models facilitate the description of target RCS characteristics and are used to quantitatively calculate radar detection probability, false alarm probability, and the required signal-to-noise ratio (SNR) for single or accumulated pulses. Commonly used fluctuation models include the Swerling model [7], chi-square model [9], log-normal model [10], and non-parametric model [11], among others.

Active cancellation technology is an advanced stealth technology based on the principle of coherent interference. It has the potential to render a target completely invisible in the direction of the radar antenna. Although achieving this in engineering is challenging, both theoretical research and practical applications have advanced rapidly in recent years [12], [13], [14], [15]. Many scholars have studied the underlying mechanisms and proposed various cancellation methods. Xiang and Qu [16] discussed the cancellation analysis of LFM interrupted continuous wave (LFM ICW) signals using the group delay and ambiguity function. Xu et al. [17] designed a cancellation system based on group delay to address LFM signal cancellation problems and proposed an active cancellation stealth system. They also investigated a scheme for NFLM signal cancellation systems [18]. Additionally, active cancellation stealth was analyzed based on interrupted-sampling and convolution modulation in [19]. Yi and Wang [20] studied the detection probability of the Swerling model before and after cancellation. In Ref. [21], they presented a method for generating the NFLM cancellation signal based on the Nth-order SSC (Spectrum Spread and Compression) algorithm. However, these studies assumed $a'_{RCS} = 1$ and $\varphi'_{RCS} = 0$ (see Eq. (2)), neglecting the target's amplitude-phase modulation of the echo signal, which does not reflect actual conditions.

In this work, we consider the target's amplitude-phase modulation of the echo signal during the design stage of the canceling signal. The canceling signals of LFM and NFLM are generated using the Nth-order SSC algorithm. The Swerling and chi-square fluctuation models are utilized to simulate the target's dynamic RCS characteristics. Besides, the discrepancies between the exact and approximate RCS fluctuation data are analyzed concerning their effect on cancellation. Finally, the corresponding detection probabilities are calculated in the subsequent sections.

II. LINEAR AND NONLINEAR FREQUENCY MODULATION SIGNAL AND CANCELLING SIGNAL

The general expression for an FM chirp signal can be given as follows:

$$u(t) = a(t) \exp [j\varphi(t)], \quad (1)$$

where $a(t)$ and $\varphi(t)$ denote the amplitude modulation function and the phase modulation function, respectively. For simplicity, we assume $a(t) = 1$ for $0 \leq t \leq T$.

In this paper, linear and two types of nonlinear frequency modulation signals are considered. Their analytical expressions are provided in Table I, where f_0 is the carrier frequency, B is the bandwidth, T is the pulse width, $A(n)$ represents the coefficients of the finite series, and $\beta = \arctan(\alpha_1)$, with $\alpha_1 \in [0, \infty)$ [22], [23], [24].

Suppose the echo signal of LFM and NLFM is

$$u_r(t) = u(t)a'_{RCS} \exp(j\varphi'_{RCS}), \quad (2)$$

where a'_{RCS} is the target's exact RCS phase and φ'_{RCS} is the amplitude. Let $\lambda' = a'_{RCS} \exp(j\varphi'_{RCS})$, then we can get

$$u_r(t) = \lambda' u(t), \quad (3)$$

where λ' satisfies the fluctuation model shown in Table III.

In Ref.[21], the authors proposed a method to generate the cancelling signal of LFM and NLFM based on Nth-order SSC algorithm. The same method will be used to generate the cancelling signal.

Suppose the cancelling signals of LFM and NLFM are that

$$u_C(t) = [u(t - \tau_0)]^N [u^*(t - \tau_0 - \tau)]^{N-1} a''_{RCS} \exp[j(\varphi''_{RCS} + \pi)], \quad (4)$$

where τ_0 is the retransmitting delay time that satisfies $\tau_0 = (N - 1)\tau$. Let $\lambda'' = \alpha''_{RCS} \exp(j\varphi''_{RCS})$, then one can obtain

$$u_C(t) = \lambda'' [u(t - \tau_0)]^N [u^*(t - \tau_0 - \tau)]^{N-1} \exp[j\pi], \quad (5)$$

where α''_{RCS} is the target's approximate RCS phase and φ''_{RCS} is the amplitude. λ'' satisfies the fluctuation model the same as λ' .

The final results of the cancelling signals of LFM and NLFM can be written as Eq.(6), the detailed derivation process may refer to the Refs. [21].

$$u_C(t) = \lambda' u(t) \exp[j\theta(\tau_0, N)], \quad (6)$$

where $\theta(\tau_0, N)$ are listed in Table II.

III. OBTAINED CANCELLING SIGNAL ANALYSIS

In this section, the obtained cancelling signal is analyzed. Given a hypothesis in the time domain, the cancelling wave synchronizes with the target echo, and a'_{RCS} , $a''_{RCS} \neq 1$, φ'_{RCS} , $\varphi''_{RCS} \neq 0$, the signal of received radar echo can be expressed as

$$u_o(t) = u_r(t) + u_C(t) = u(t) \{ \lambda' + \lambda'' \exp [j\theta(\tau_0, N)] \}. \quad (7)$$

In the vast majority case, $\lambda' \neq \lambda''$, but if one has

$$\lambda'' = \delta \cdot \lambda', \quad (8)$$

where λ is called the errors between the exact and approximate RCS fluctuation data. Then

$$u_o(t) = \lambda' u(t) \{ 1 + \delta \exp [j\theta(\tau_0, N)] \}. \quad (9)$$

After matching filter, one can get

$$u_\sigma(t) = u_o(t) * h(t) = \lambda' \{ 1 + \delta \exp [j\theta(\tau_0, N)] \} u(t) * h(t). \quad (10)$$

Let

$$\gamma = |1 + \delta \exp [j\theta(\tau_0, N)]|, \quad (11)$$

the cancellation effect is related to the magnitude of γ . Cancellation effect does not exist when $\gamma = 1$, the cancelling wave has cancellation effect when $\gamma < 1$. And the radar echo will be strengthened by the cancelling wave when $\gamma > 1$.

In Ref. [21], the authors discussed the cancellation effect with $\delta = 1$ for various values of N and τ_0 . This section extends the discussion to the cancellation effect for $\delta \neq 1$.

In the analysis, the pulse width is set to $T = 50 \mu s$, $\beta = 1.4$, and the bandwidth $B = 10$ MHz. The variation of the cancellation coefficient γ for LFM, Taylor window-based NLFM, and tangent-based NLFM with respect to δ is shown in Figs. 1, 2, and 3, respectively, for different values of N and τ_0 .

It can be observed that the cancellation signal suppresses the radar echo for $\delta \neq 1$, including cases where $\delta > 1$. This indicates that effective cancellation can still be achieved even when there are discrepancies between the target's exact RCS and its approximate RCS. From Figs. 1a and 3a, the radar echo is suppressed by the cancellation signal when $\delta \rightarrow 1.8$ (representing significant errors) by adjusting the order N for both LFM and tangent-based NLFM. However, this condition requires $\tau_0 < 2 \mu s$ (a very small value). The curves in Figs. 2b and 3b demonstrate that the radar echo is canceled by the cancellation signal only when $\delta < 1$ for certain values of N . Additionally, for LFM, effective cancellation occurs with larger τ_0 and δ , as illustrated in Fig. 1.

IV. RADAR DETECTION PROBABILITY FOR SOME FLUCTUATING TARGET CASES

The fluctuation of the target's RCS will reduce its detection performance. To measure the influence of the fluctuation on the detection probability, the target RCS fluctuation characteristic needs to be described. It is difficult to accurately obtain the probability distribution function of each target's RCS as their complex shape structures and diversity. The usual approach is to utilize a reasonable distribution model to investigate the impact of target fluctuation on radar detection performance. Plenty of researching work had been done and classical models like Swerling model, chi-square model etc. had been widely utilized. Table III introduces the classical distribution model and their probability density functions in accordance with the development sequence of the existing model.

In previous studies of radar detection theory, the target's RCS was usually considered constant. However, for a target in the optical zone, especially aircraft with edges, corners, cavities, etc., the RCS rapidly changes with the shape and surface roughness of the target, implying a non-fixed RCS. The impact of RCS fluctuation must be considered when studying radar detection theory for such targets.

As discussed in the research literature, the Swerling model is a special case of the chi-square model. The detection probability of the chi-square model can be used to calculate the radar target's detection probability. The detection probability

TABLE I: The expressions of Linear and nonlinear frequency modulation signal

LFM signal	$u(t) = \exp[j2\pi(f_0t + \mu t^2/2)]$
Taylor window waveform NLFM signal	$u(t) = \exp \left[j \left(\frac{\pi B t^2}{T} + 2BT \sum_{n=1}^5 \frac{A(n)}{n} \sin^2 \left(\frac{\pi n t}{T} \right) \right) \right]$
Tangent-based waveform NLFM signal	$u(t) = \exp \left[-j \frac{\pi B T}{2\beta \tan \beta} \ln \left \cos \left(2\beta \frac{t}{T} \right) \right \right]$

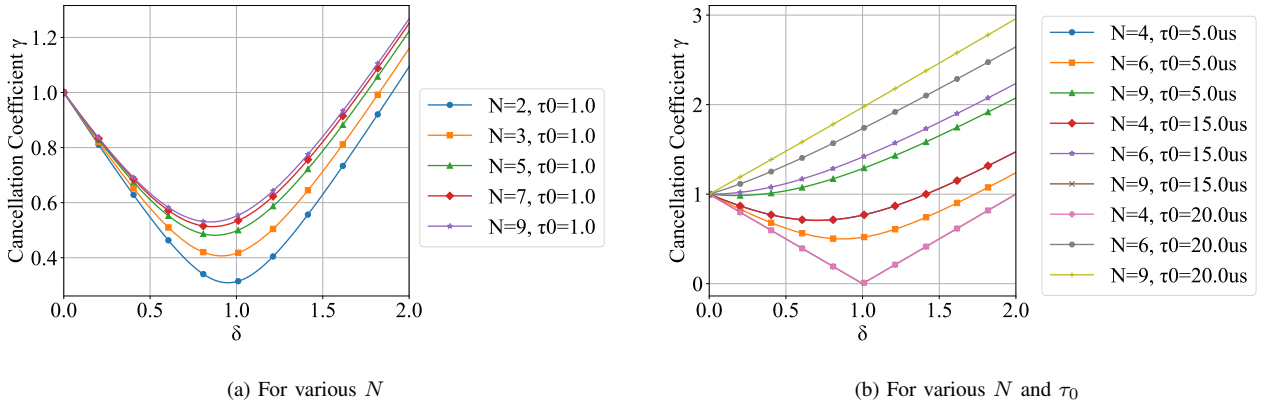


Fig. 1: Cancellation coefficient versus δ for different N, τ_0 (LFM)

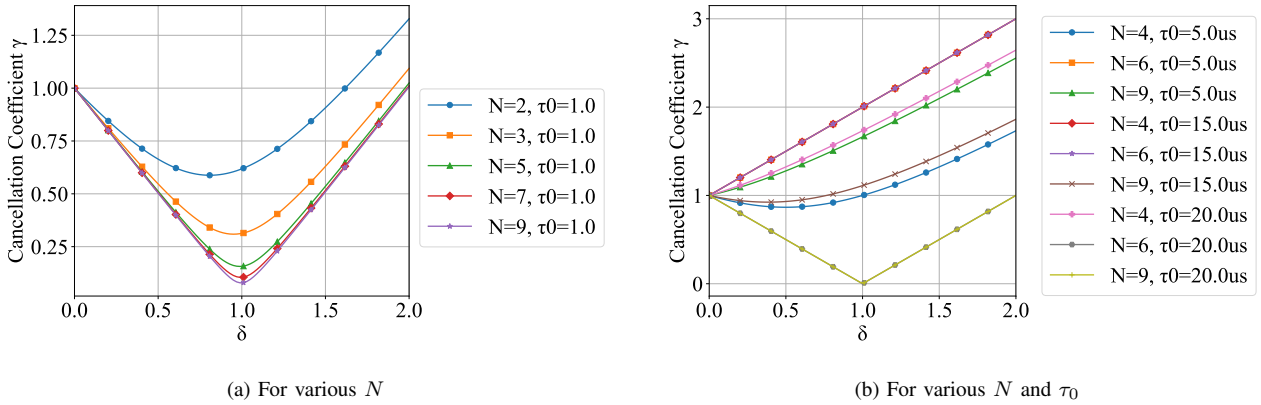


Fig. 2: Cancellation coefficient versus δ for different N, τ_0 (Taylor window NLFM)

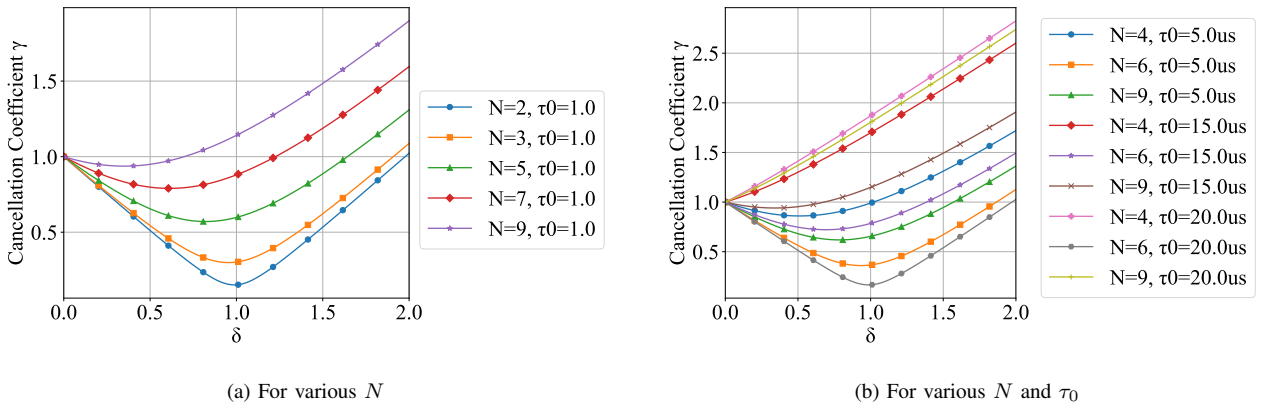


Fig. 3: Cancellation coefficient versus δ for different N, τ_0 (Tangent-based NLFM)

TABLE II: A The specific expressions of $\theta(\tau_0, N)$

LFM signal	$\theta(\tau_0, N) = \pi\mu\tau_0^2 \left(1 - \frac{1}{N}\right) + \pi$
Taylor window waveform NLFM signal	$\theta(\tau_0, N) = -\frac{\pi B}{T} \frac{N\tau_0^2}{N-1} + \pi + 2BT \sum_{n=1}^5 \frac{A(n)}{n} \left((N-1) \sin\left(\frac{\pi n}{T} \frac{\tau_0}{N-1}\right) - \sin\left(\frac{\pi n \tau_0}{T}\right) \right)$
Tangent-based waveform NLFM signal	$\theta(\tau_0, N) = \frac{\pi BT}{2\beta \tan(\beta)} \left((N-1) \ln \left \cos\left(\frac{2\beta}{T} \frac{\tau_0}{N-1}\right) \right \right) - \ln \left \cos\left(\frac{2\beta \tau_0}{T}\right) \right + \pi + \frac{\pi BT}{2\beta \tan(\beta)} \left((N-1) \ln \left 1 + \tan\left(\frac{2\beta}{T} \frac{\tau_0}{N-1}\right) \right \right) - \ln \left 1 + \tan\left(\frac{2\beta \tau_0}{T}\right) \right $

TABLE III: Typical RCS fluctuation model

Model	Probability density function
Swerling I-II model	$f(\sigma) = \frac{1}{\sigma} \exp\left(-\frac{\sigma}{\bar{\sigma}}\right), \sigma \geq 0$
Swerling III-IV model	$f(\sigma) = \frac{4\sigma}{\bar{\sigma}^2} \exp\left(-\frac{2\sigma}{\bar{\sigma}}\right), \sigma \geq 0$
Chi-square model with $2k$ degree of freedom	$f(\sigma) = \frac{k}{(k-1)! \bar{\sigma}} \left(\frac{k\sigma}{\bar{\sigma}}\right)^{k-1} \exp\left(-\frac{k\sigma}{\bar{\sigma}}\right), \sigma \geq 0$

P_D for single pulse detection can be expressed as follows [25]:

$$P_D = \int_0^\infty \int_{r_b}^\infty p(A) \cdot r \exp\left(-\frac{r^2 + SNR}{2}\right) I_0(r\sqrt{SNR}) dr dA, \quad (12)$$

where $r_b = \sqrt{2 \ln \frac{1}{P_{fa}}}$ is the threshold, P_{fa} is the false alarm probability, and $p(A)$ is the probability density function of the amplitude of the backscattering pulse, which can be computed as [26]:

$$cp(A) = \left(\frac{kA}{\Gamma(k)m\bar{\sigma}}\right)^{k-1} \exp\left(-\frac{kA^2}{2m\bar{\sigma}}\right), \quad A > 0, \quad (13)$$

where m is a constant depending on the radar system's working parameters, such as transmitting power, antenna gain, etc., and the distance R . The SNR in Eq. (12) is the signal-to-noise ratio and can be calculated as:

$$SNR = \frac{2E}{N_0}, \quad (14)$$

where E is the signal energy and $N_0/2$ is the two-sided white Gaussian noise spectral density.

The detection probability P_D for non-coherent pulse accumulation detection can be written as follows [27]:

$$P_D = \int_0^\infty \int_{V_T}^\infty p(A) \cdot \left(\frac{2r}{n \cdot SNR}\right)^{\frac{n-1}{2}} \exp\left(-r - \frac{n \cdot SNR}{2}\right) I_{n-1}(\sqrt{2n \cdot SNR}) dr dA, \quad (15)$$

where V_T is the detection threshold. When the false alarm probability P_{fa} is given, the threshold can be solved by Eq.(16) as follows

$$P_{fa} = \int_{V_T}^\infty \frac{x^{n-1} \exp(-x)}{(n-1)!} dx. \quad (16)$$

where V_T is the detection threshold. When the false alarm probability P_{fa} is given, the threshold can be solved using Eq. (16) as follows:

$$P_{fa} = \int_{V_T}^\infty \frac{x^{n-1} \exp(-x)}{(n-1)!} dx. \quad (17)$$

Calculating the radar target detection probability provides a reference for radar target detection practice. To facilitate engineering practice, researchers have derived approximate

formulations of detection probability for different fluctuating models through mathematical approximation and experience, greatly improving calculation speed while maintaining accuracy. Table IV shows the approximate formulations of detection probability for different fluctuating models [28], [29]. In Table IV, $\Gamma_1(x, N) = \int_0^x \frac{\exp(-v)v^{N-1}}{(N-1)!} dv$ is the incomplete gamma function, and \bar{S} is the mean of SNR S_i , which conforms to the chi-square model with $2k$ degrees of freedom. The subsequent calculation of detection probability will be performed using these approximate formulations.

V. THE EFFECT OF CANCELLATION ON THE DETECTION PROBABILITY

As we all know, active cancellation can significantly reduce the echo gain. According to the interference principle of coherent waves, the radar echo can be completely cancelled out when the following conditions are satisfied [30]:

- In the time domain, the echo should be synchronized with the peak point of the signal.
- The echo and the peak point of the signal need to be in opposite phases for cancellation.
- The amplitude of the echo and the peak point of the signal should be equal for cancellation.

Even with some errors in amplitude, phase, and frequency, there is still a cancellation effect[21]. Next, we will primarily discuss the influence of RCS fluctuation errors on the cancellation effect, based on radar detection probability.

A. Swerling model distribution

If λ' in Eq. (2) conforms to the Swerling model, its probability density function can be obtained from Table III. Using Eq. (10), the improved SNR after cancellation can be approximately derived as

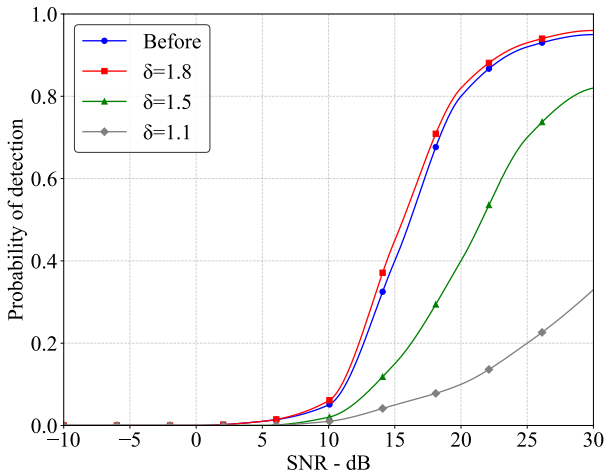
$$SNR_L = |1 + \delta \exp[j\theta(\tau_0, N)]| \cdot SNR. \quad (18)$$

By combining Eq. (17) with Tables II and IV, we can obtain the detection probability curves for LFM and NLFM signals versus SNR for different cases.

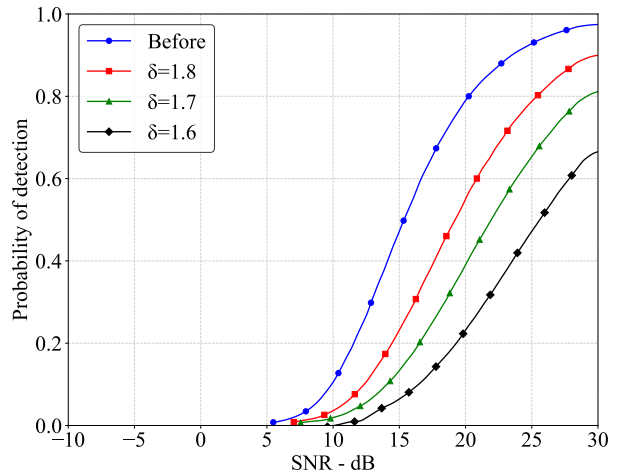
- 1) **LFM Case:** Fig. 4 and Fig. 5 illustrate the detection probability (P_D) curves for LFM signals versus signal-to-noise ratio (SNR) under the Swerling I target model for various values of δ . These results indicate that the cancelling signal effectively reduces P_D , with the suppression effect becoming more pronounced as δ

TABLE IV: The approximate formulations of detection probability

Model	Detection probability
Swerling III model	$P_D = \begin{cases} \exp[-V_T/(1 + \text{SNR})], & n = 1 \\ 1 - \Gamma_1(V_T, n - 1) + (1 + \frac{1}{n \cdot \text{SNR}})^{n-1} \Gamma_1\left(\frac{V_T}{1 + \frac{1}{n \cdot \text{SNR}}}, n - 1\right) \\ \quad \times \exp[-V_T/(1 + n \cdot \text{SNR})], & n > 1 \end{cases}$ $P_{fa} = 1 - \Gamma_1(V_T, n - 1)$ $\Gamma_1(x, N) = \int_0^x \frac{\exp(-v)v^{N-1}}{(N-1)!} dv.$
Swerling III-IV model	$P_D = \exp\left(\frac{-V_T}{1+n \cdot \text{SNR}/2}\right) \left(1 + \frac{2}{n \cdot \text{SNR}}\right)^{n-2} \times K_0, \quad n = 1, 2$ $K_0 = 1 + \frac{V_T}{1+n \cdot \text{SNR}/2} - \frac{2(n-2)}{n \cdot \text{SNR}}$ $P_D = \frac{V_T^{n-1} \exp(-V_T)}{(1+n \cdot \text{SNR}/2)(n-2)!} + 1 - \Gamma_1(V_T, n - 1) + K_0 \times \Gamma_1\left(\frac{V_T}{1+2/n \cdot \text{SNR}}, n - 1\right), \quad n > 2$
Chi-square model with $2k$ degree of freedom	$P_D = A_1 + A_2 + A_3$ $A_1 = \left[1 + \frac{k}{n \cdot S}\right]^{n-k} \left[1 - I\left(\frac{Z_b}{\sqrt{k}}, k - 1\right)\right]$ $A_2 = \frac{\left[1 + \frac{k}{n \cdot S}\right]^{n-k+1} (n-k)}{\left[1 + \frac{n \cdot S}{k}\right]} \left[\frac{e^{-Z_b} Z_b^{k-1}}{\Gamma(k)} - (1 - I)\right]$ $A_3 = \frac{\left[1 + \frac{k}{n \cdot S}\right]^{n-k+2} (n-k)(n-k+1)}{2\left[1 + \frac{n \cdot S}{k}\right]^2} \left[(1 - I) - \frac{e^{-Z_b} Z_b^{k-2}}{\Gamma(k-1)} - \frac{e^{-Z_b} Z_b^{k-1}}{\Gamma(k)}\right]$ $Z_b = \frac{V_T}{\left[1 + \frac{n \cdot S}{k}\right]}$ $I(p, q) = \int_0^p \sqrt{1+q} \frac{e^{-v} v^q}{q!} dv$



(a) $\tau_0 = 1\mu s, N = 3$



(b) $\tau_0 = 20\mu s, N = 4$

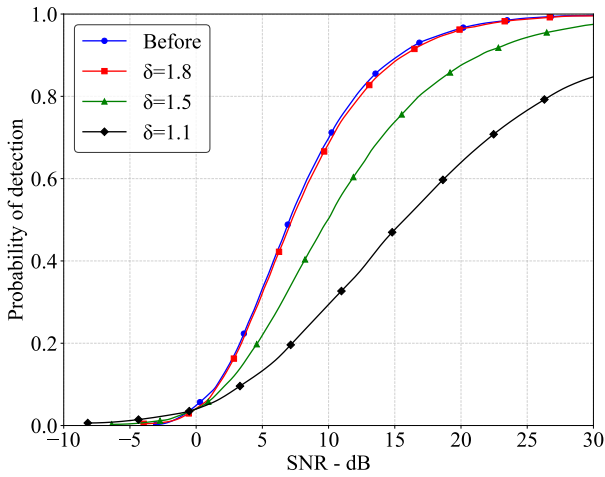
Fig. 4: P_D versus SNR for Swerling I type target with different δ (LFM, $P_{fa} = 10^{-11}, n = 1$)

decreases. When comparing subfigures 4a and 5a with 4b and 5b, it becomes evident that by appropriately adjusting the cancellation order N , the radar echo can be cancelled even when δ and τ_0 are large. Furthermore, the comparison between Fig. 4 and Fig. 5 demonstrate that the cancellation effect diminishes with increasing n . However, this attenuation can be mitigated or even reversed by controlling δ . These results highlight the flexibility and robustness of the cancellation approach for LFM signals under varying conditions.

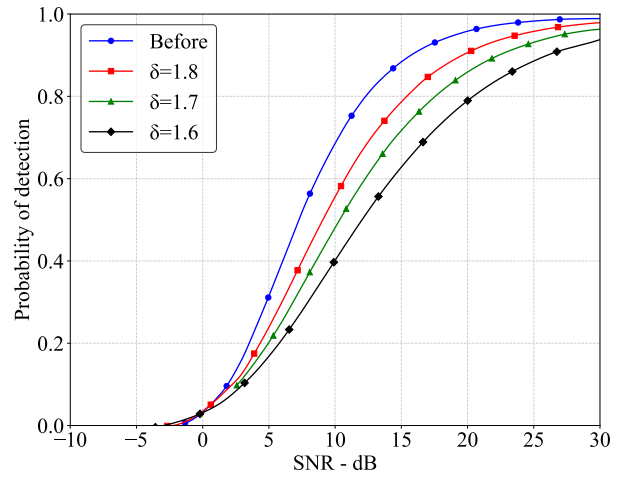
2) **Taylor Window NLFM Case:** Fig. 6 and Fig. 7 depict the detection probability curves for Taylor window-based NLFM signals as a function of SNR, evaluated under the Swerling I target model with different δ values. These figures confirm that the cancelling signal achieves significant suppression of radar echoes across a wide range of parameters, including τ_0 , δ , and n . A detailed examination of Fig. 6a, Fig. 7a, Fig. 6b,

and Fig. 7b reveal that the cancellation effect is particularly strong when $\tau_0 = 1\mu s$, which aligns closely with real-world radar systems. Additionally, from Fig. 6b and Fig. 7b, it is evident that the radar echo is effectively suppressed only when $\delta < 1$, and the effectiveness decreases as n increases. These results emphasize the importance of parameter optimization in Taylor window-based NLFM signal cancellation to achieve optimal stealth performance.

3) **Tangent-Based NLFM Case:** Fig. 8 and Fig. 9 show the detection probability curves for tangent-based NLFM signals versus SNR, evaluated under the Swerling III target model for various δ values. From Fig. 8a, it is observed that P_D is minimized when $\tau_0 = 2\mu s$ and $\delta = 1.2$, achieving a 0.3 reduction in detection probability. Compared to LFM and Taylor window NLFM cases, tangent-based NLFM signals exhibit the most significant suppression of P_D , with reductions

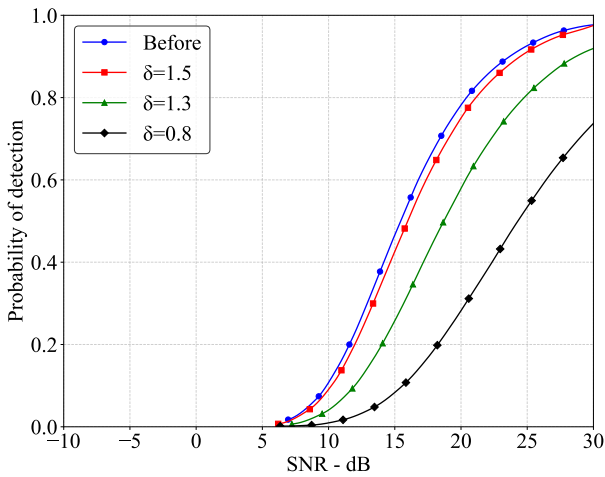


(a) $\tau_0 = 1\text{us}, N = 3$

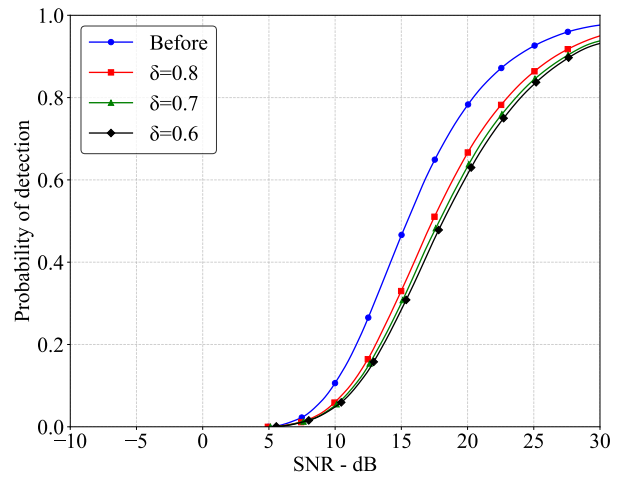


(b) $\tau_0 = 20\text{us}, N = 4$

Fig. 5: P_D versus SNR for Swerling I type target with different δ (LFM, $P_{fa} = 10^{-11}, n = 10$)



(a) $\tau_0 = 1\text{us}, N = 9$



(b) $\tau_0 = 20\text{us}, N = 9$

Fig. 6: P_D versus SNR for Swerling I type target with different δ (Taylor window LFM, $P_{fa} = 10^{-11}, n = 1$)

reaching up to 0.7. This observation underscores the potential of tangent-based NLFM cancellation signals to achieve complete radar stealth. However, the remaining subfigures indicate that achieving such significant reductions requires stringent conditions, particularly precise control of δ and τ_0 . These results highlight the high sensitivity and performance potential of tangent-based NLFM signals for stealth applications, albeit with stricter design requirements.

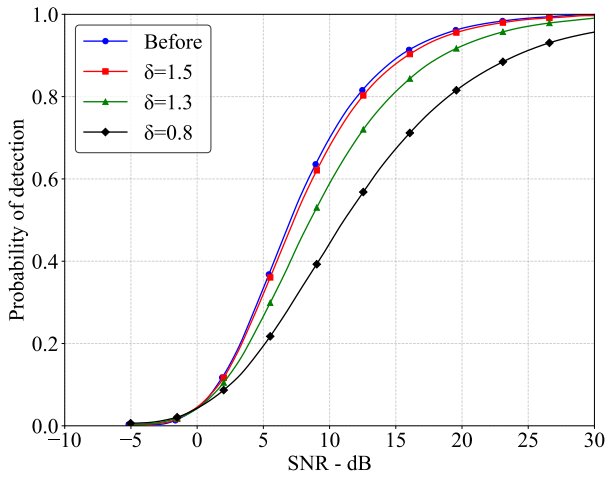
B. Chi-square distribution

In this section, computational models representing stealth aircraft types I and II were employed. Their geometric configurations, designed using CATIA, are depicted in Figs. 10 and 11. Subsequently, these models were meshed using HyperMesh and imported into FEKO for RCS analysis, where their RCS followed the chi-square distribution. By fitting their probability density curves and resolving the

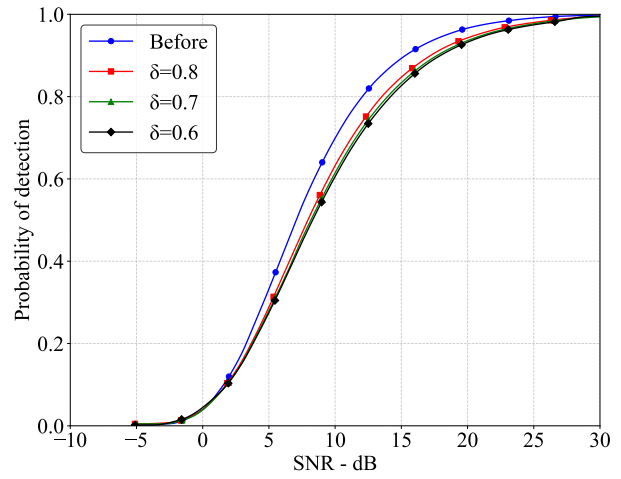
degrees of freedom, the probability density function was determined using Table III.

Utilizing Eq. (17), along with data from Table II and Table IV, enabled the derivation of detection probability curves for LFM and NLFM signals versus SNR for different stealth aircraft.

- 1) LFM Case: Fig. 12 and Fig. 13 illustrate the detection probability (P_D) curves for LFM signals versus SNR, evaluated for chi-square model stealth aircraft I with varying values of τ_0, N , and $n_{fa} = 10^{10}$. Here, n_{fa} is a parameter that determines the false alarm probability (P_{fa}) in radar signal processing. In the context of this study, it signifies an extremely high false alarm threshold, chosen to illustrate system performance under minimal P_{fa} conditions. The results clearly show that the cancelling signals can significantly reduce P_D , even for $\delta = 1.5$. When the fitted probability density curves closely align with the exact RCS values, the cancelling signals effectively nullify the echo signals,

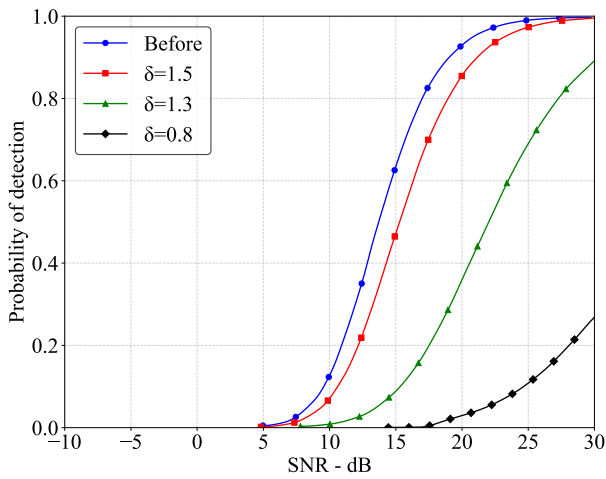


(a) $\tau_0 = 1\mu s, N = 9$

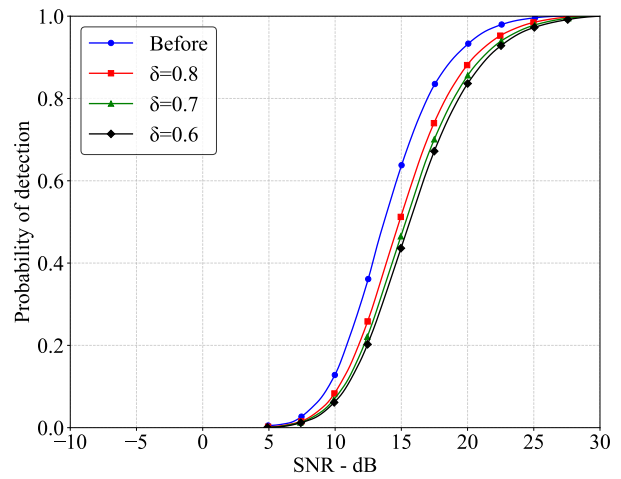


(b) $\tau_0 = 20\mu s, N = 9$

Fig. 7: P_D versus SNR for Swerling I type target with different δ (Taylor window LFM, $P_{fa} = 10^{-11}, n = 10$)

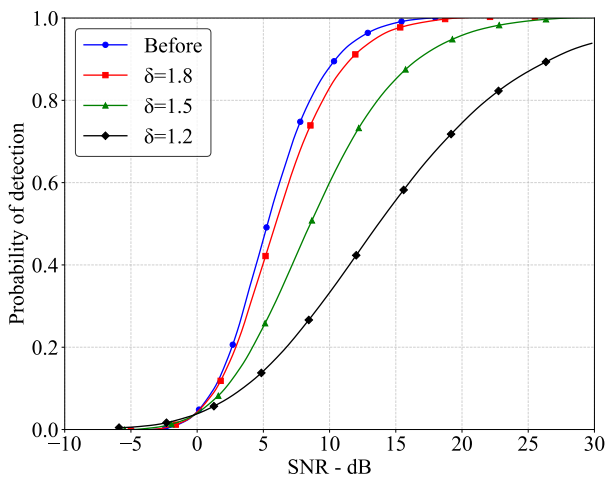


(a) $\tau_0 = 2\mu s, N = 3$

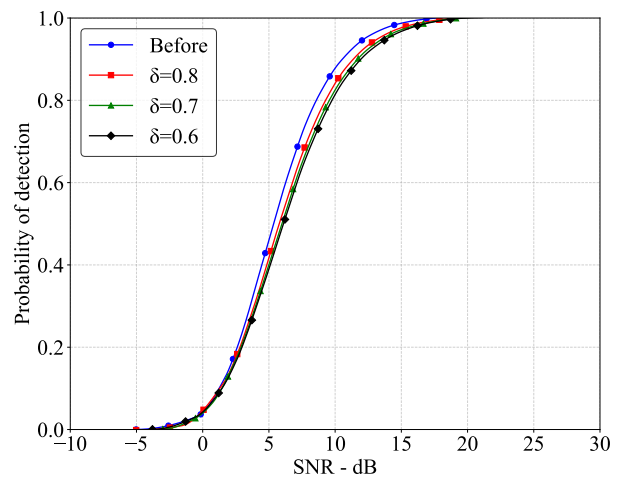


(b) $\tau_0 = 20\mu s, N = 6$

Fig. 8: P_D versus SNR for Swerling III type target with different δ (Tangent-based LFM, $P_{fa} = 10^{-11}, n = 10$)



(a) $\tau_0 = 2\mu s, N = 3$



(b) $\tau_0 = 20\mu s, N = 6$

Fig. 9: P_D versus SNR for Swerling III type target with different δ (Tangent-based LFM, $P_{fa} = 10^{-11}, n = 10$)

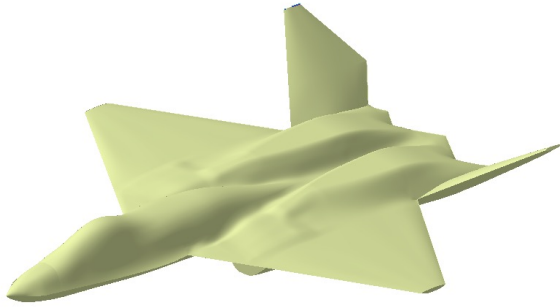


Fig. 10: Stealth aircraft I.

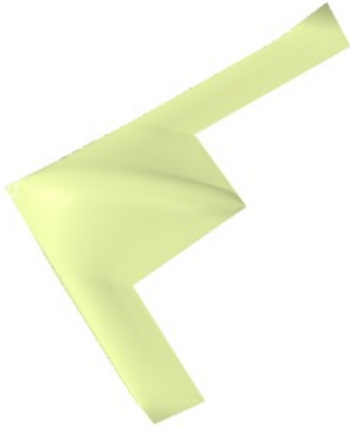


Fig. 11: Stealth aircraft II.

achieving substantial suppression of detection probability. Moreover, the proposed cancelling signals demonstrate resilience against inaccuracies in the numerical RCS, maintaining their ability to cancel radar echoes despite discrepancies from the exact RCS values. A deeper analysis of Fig. 12b and Fig. 13b highlight that the cancellation effect becomes more pronounced as τ_0 and n increase. This suggests that the cancellation mechanism is particularly effective under conditions of larger delay times and higher numbers of accumulated pulses. Such findings underline the potential of active cancellation technology to enhance the stealth performance of stealth aircraft I across a wide range of operational scenarios, making it a versatile tool for reducing radar detectability.

- 2) Taylor Window Waveform NLFM Case: Fig. 14 and Fig. 15 depict detection probability (P_D) surfaces for Taylor window-based NLFM signals as functions of SNR and azimuth, analyzed for chi-square model stealth aircraft II under various values of δ , τ_0 , and n . These results reveal that the P_D surfaces after cancellation are consistently lower than those before cancellation, irrespective of the parameter combinations. This reduction in P_D spans a broad range of SNR levels and azimuth angles, underscoring the effectiveness of the proposed cancellation approach. The cancelling signals exhibit a remarkable ability to suppress radar echoes across all azimuth angles, effectively achieving omnidirectional stealth for stealth aircraft II. This capability demonstrates the robustness of active cancellation technology, making it suitable for a variety of tactical environments.

A comparison of Fig. 14a and Fig. 14b indicate that for larger τ_0 values, successful cancellation is achieved only when $\delta < 1$. This suggests that controlling δ is critical for maintaining effective cancellation at larger delay times. Furthermore, the effectiveness of cancellation diminishes as the number of pulse accumulations increases, making smaller values of δ necessary for optimal performance. Despite potential inaccuracies in the target's RCS, the cancelling signals designed in this study continue to enhance the stealth performance of stealth aircraft II. This robustness highlights the practical value of the proposed methodology, ensuring consistent performance even under conditions of RCS fluctuation or modeling error. These findings reinforce the feasibility of active cancellation as a key strategy for reducing radar detectability in both linear and nonlinear frequency modulation scenarios. The ability to achieve significant reductions in detection probability across different models and parameters makes this approach a promising candidate for advancing stealth technologies.

C. Mixed Distribution Model Analysis

To provide a more comprehensive analysis of radar detection probability under realistic conditions, we developed a mixed distribution model that combines the characteristics of Swerling I, Swerling III, and chi-square distributions. The probability density function of this mixed model is given by:

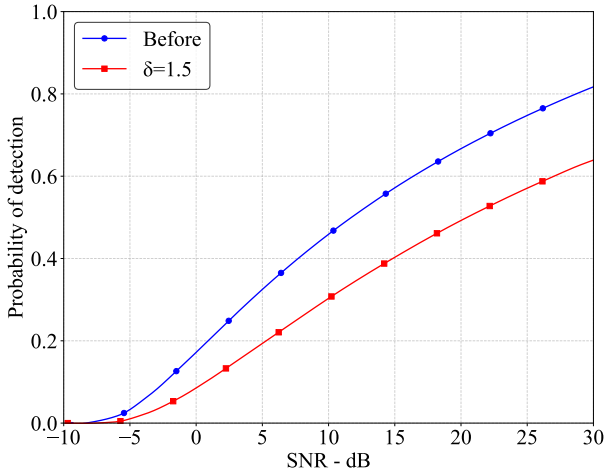
$$f_{mixed}(\sigma) = w_1 f_{SI}(\sigma) + w_2 f_{SIII}(\sigma) + w_3 f_{\chi^2}(\sigma) \quad (19)$$

where w_1 , w_2 , and w_3 are weighting coefficients satisfying $\sum_{i=1}^3 w_i = 1$, and f_{SI} , f_{SIII} , and f_{χ^2} are the probability density functions of Swerling I, Swerling III, and chi-square distributions respectively.

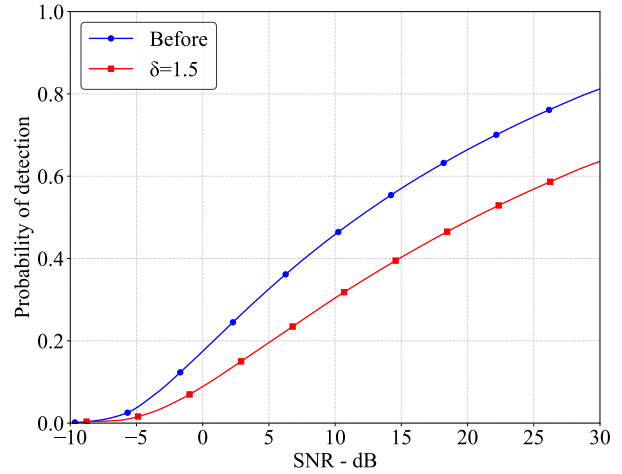
Fig. 16 and Fig. 17 present the detection probability curves for different false alarm probabilities P_{fa} and pulse numbers n , with varying cancellation factors δ . For single-pulse detection $n = 1$, as shown in Fig. 16a and Fig. 17a, the cancellation method effectively reduces the detection probability across all SNR values. The reduction is most pronounced when $\delta = 0.8$, where we observe a substantial rightward shift in the detection probability curve, indicating that a higher SNR is required to achieve the same detection probability as before cancellation.

With increased pulse accumulation ($n = 5$), depicted in Fig. 16b and Fig. 17b, the overall detection probability improves for all cases due to the coherent integration gain. However, the cancellation effect remains significant, particularly for $\delta = 0.8$ and $\delta = 1.3$. Notably, under $P_{fa} = 10^{-2}$, we observe a unique oscillatory behavior in the detection probability curves for $n = 5$ (Fig. 16b), suggesting a complex interaction between pulse accumulation and cancellation effects.

The comparison of results under different false alarm probabilities reveals that stricter requirements ($P_{fa} = 10^{-6}$ versus $P_{fa} = 10^{-2}$) lead to several key observations. A rightward shift occurs in all detection probability curves, indicating higher SNR requirements. There is more pronounced separation between curves with different δ values. The cancellation effects become more stable and predictable, particularly evident in the absence of oscillatory behavior in Fig. 17b compared to Fig. 16b.

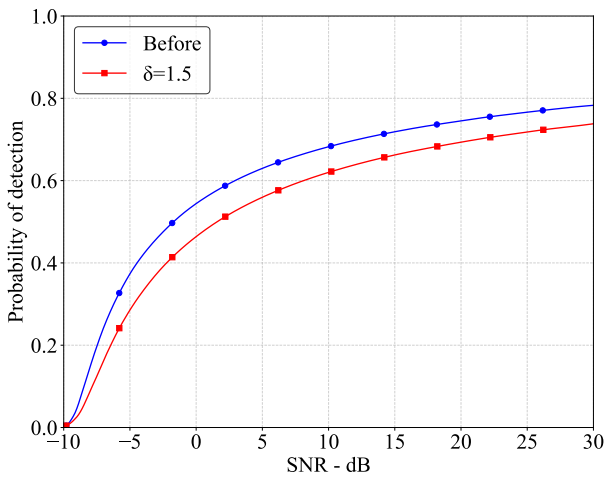


(a) $\tau_0 = 1\mu s, N = 3$

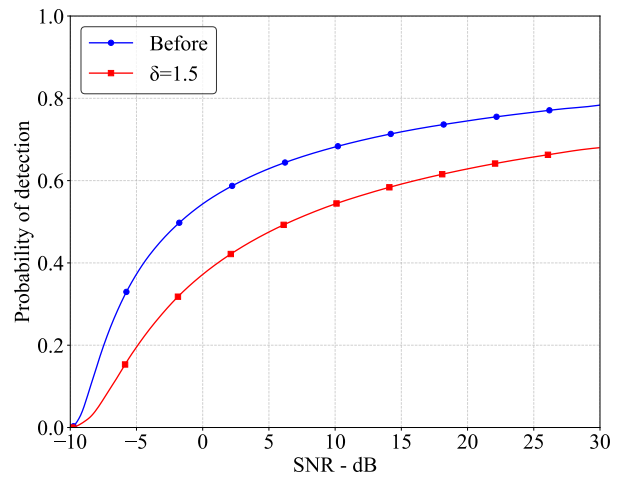


(b) $\tau_0 = 20\mu s, N = 4$

Fig. 12: P_D versus SNR for chi-square model stealth aircraft I(LFM, $n_{fa} = 10^{10}, n = 1$)

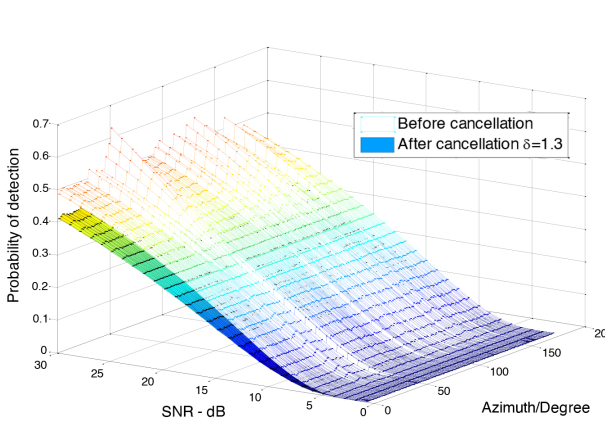


(a) $\tau_0 = 1\mu s, N = 3$

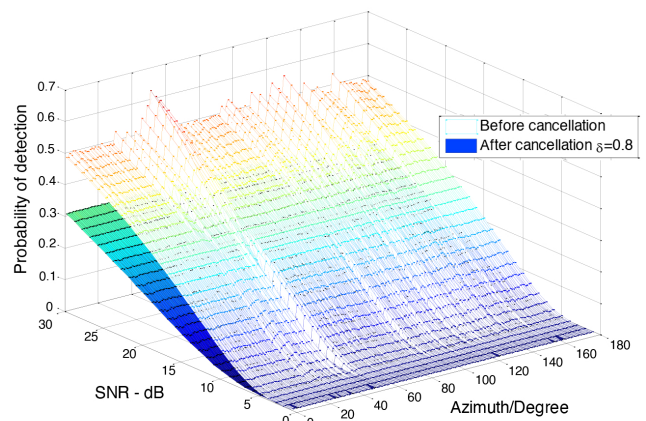


(b) $\tau_0 = 20\mu s, N = 4$

Fig. 13: P_D versus SNR for chi-square model stealth aircraft I(LFM, $n_{fa} = 10^{10}, n = 10$)



(a) $\tau_0 = 1ms, N = 9$



(b) $\tau_0 = 20ms, N = 4$

Fig. 14: P_D versus SNR, azimuth for chi-square model stealth aircraft II (Taylor window NLFM, $n_{fa} = 10^{10}, n = 1$)

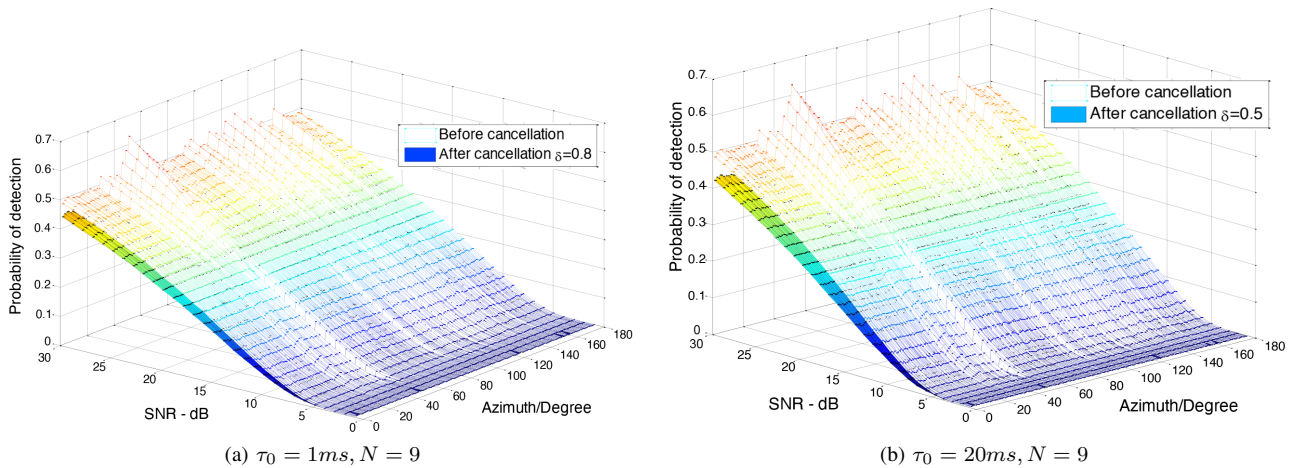


Fig. 15: P_D versus SNR, azimuth for chi-square model stealth aircraft II (Taylor window NLFM, $n_{fa} = 10^{10}, n = 10$)

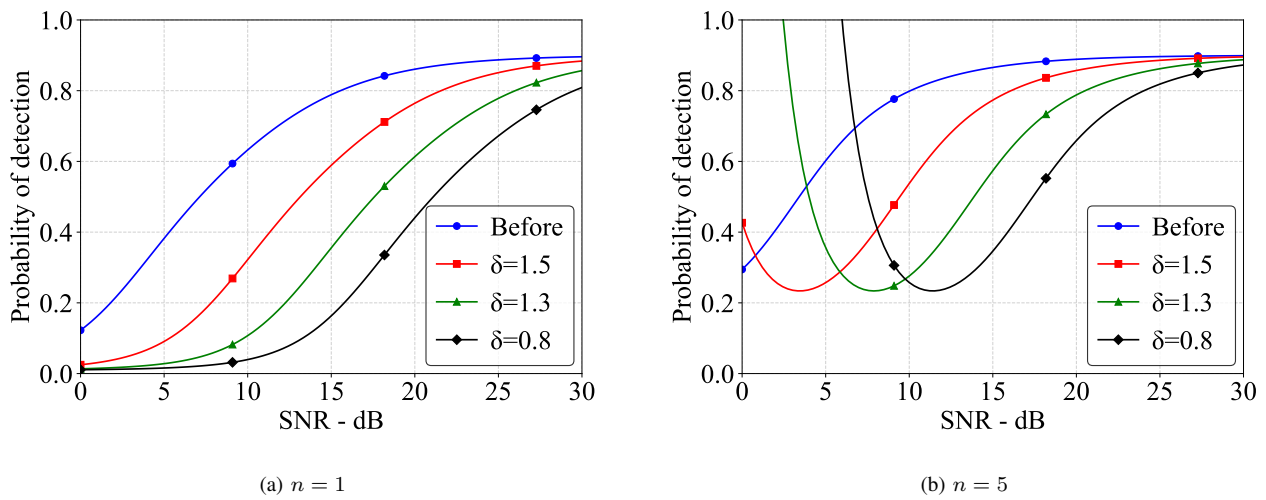


Fig. 16: P_D versus SNR for for the mixed distribution model under $P_{fa} = 10^{-2}$.

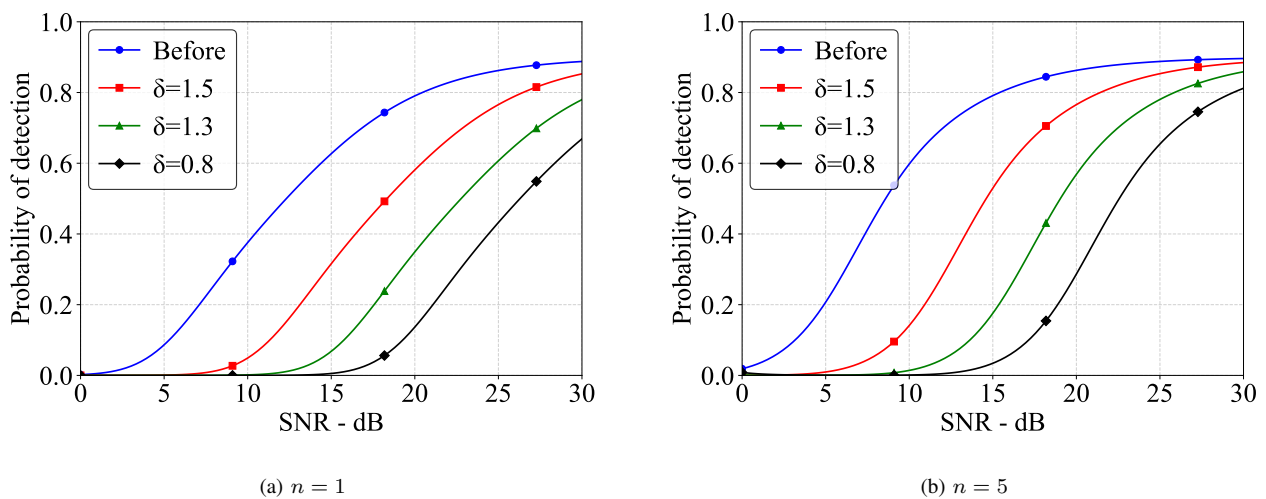


Fig. 17: P_D versus SNR for for the mixed distribution model under $P_{fa} = 10^{-6}$.

The experimental results confirm that our cancellation method maintains its effectiveness even under this more realistic mixed distribution model. The system demonstrates robust performance across various operational parameters, with the most effective cancellation achieved at $\delta = 0.8$, suggesting that slight under-cancellation may be preferable to over-cancellation in practical applications.

VI. CONCLUSION

The cancelling signals generated for LFM and NLFM signals through the N th-order SSC algorithm, accounting for the target's amplitude-phase modulation, effectively mitigate the target echo. Remarkably, this cancellation effect persists even when errors are present ($\delta \neq 1$). By appropriately selecting the order N and controlling the error δ , the detection probability for RCS fluctuation models indicates a reduction at large delay times. Moreover, for non-coherent pulse accumulation detection, the cancelling signals continue to nullify the echo signals under certain error conditions. These proposed cancelling signals are well-suited for engineering applications, accommodating large delay times and errors. Importantly, the implementation of active cancellation technology paves the way for achieving omnidirectional stealth capabilities for stealth aircraft.

REFERENCES

- [1] B. R. Mahafza, *Radar systems analysis and design using MATLAB*. Chapman and Hall/CRC, 2005.
- [2] E. F. Knott, J. F. Schaeffer, and M. T. Tuley, *Radar cross section*. SciTech Publishing, 2004.
- [3] C. Cook, *Radar signals: An introduction to theory and application*. Elsevier, 2012.
- [4] A. Jain and I. Patel, "Dynamic imaging and rcs measurements of aircraft," *IEEE transactions on aerospace and electronic systems*, vol. 31, no. 1, pp. 211–226, Jan. 1995.
- [5] W. du Preez and J. van Schalkwyk, "Processing of dynamic radar cross section measurements," in *Proceedings of the 1992 South African Symposium on Communications and Signal Processing*, Aug, 1992, pp. 29–32.
- [6] J. Marcum, "A statistical theory of target detection by pulsed radar," *IRE Transactions on Information Theory*, vol. 6, no. 2, pp. 59–267, Apr. 1960.
- [7] P. Swerling, "Radar probability of detection for some additional fluctuating target cases," *IEEE Transactions on Aerospace and Electronic Systems*, vol. 33, no. 2, pp. 698–709, Apr. 1997.
- [8] H. Karkera, S. K. Shettigar, and N. N. Katagi, "A comparative study of two wavelet-based numerical schemes for the solution of nonlinear boundary value problems," *IAENG International Journal of Applied Mathematics*, vol. 54, no. 9, pp. 1894–1904, 2024.
- [9] W. W. Weinstock, *Target cross section models for radar systems analysis*. University of Pennsylvania, 1964.
- [10] G. R. Heidbreder and R. L. Mitchell, "Detection probabilities for log-normally distributed signals," *IEEE Transactions on Aerospace and Electronic Systems*, vol. AES-3, no. 1, pp. 5–13, Jan. 1967.
- [11] X. Xu and P. Huang, "A new rcs statistical model of radar targets," *IEEE Transactions on Aerospace and Electronic Systems*, vol. 33, no. 2, pp. 710–714, Apr. 1997.
- [12] D. M. Cowell and S. Freear, "Separation of overlapping linear frequency modulated (lfm) signals using the fractional fourier transform," *IEEE Transactions on Ultrasonics, Ferroelectrics, and Frequency Control*, vol. 57, no. 10, pp. 2324–2333, 2010.
- [13] Z. Zhao and X. Shi, "Fm interference suppression for pre-cw radar based on adaptive stft and time-varying filtering," *Journal of Systems Engineering and Electronics*, vol. 21, no. 2, pp. 219–223, 2010.
- [14] J. Wang, L. Bai, Z. Fang, R. Han, J. Wang, and J. Choi, "Age of information based urllc transmission for uavs on pylon turn," *IEEE Transactions on Vehicular Technology*, vol. 73, no. 6, pp. 8797–8809, 2024.
- [15] C. Yan, L. Fu, J. Zhang, and J. Wang, "A comprehensive survey on uav communication channel modeling," *IEEE Access*, vol. 7, pp. 107 769–107 792, 2019.
- [16] Y. C. Xiang, C. W. Qu, H.-P. Hou, and Y.-K. Chen, "Analysis of lfm cancellation based on group delay and ambiguity function," *Journal of China Academy of Electronics and Information Technology*, vol. 6, no. 2, pp. 175–180, Jul. 2011.
- [17] X. Sheng and X. Yuan ming, "Design of lfm cancelling system based on group delay," *Optik*, vol. 126, no. 4, pp. 382–385, Feb. 2015.
- [18] S. Xu and Y.-m. Xu, "Scheme for nonlinear frequency modulated signal cancelling system," *Optik*, vol. 124, no. 21, pp. 4896–4900, Nov. 2013.
- [19] Q. Huang and Y. Xu, "Active cancellation stealth analysis based on interrupted-sampling and convolution modulation," *Optik*, vol. 127, no. 7, pp. 3499–3503, Apr. 2016.
- [20] M. Yi, L. Wang, and J. Huang, "Active cancellation analysis based on the radar detection probability," *Aerospace Science and Technology*, vol. 46, pp. 273–281, Oct. 2015.
- [21] M. Yi, J. Huang, and Z. Meng, "A cancelling method based on nth-order ssc algorithm for solving active cancellation problems," *Aerospace Science and Technology*, vol. 71, pp. 264–271, Dec. 2017.
- [22] W. Yu Jun, Z. Guo Qing, and W. Hong Wei, "Echo cancelling algorithm for the lfm radar," *Journal of Xidian University*, vol. 35, no. 6, pp. 1031–1035, Dec. 2008.
- [23] P. Yichun, P. Shirui, Y. Kefeng, and D. Wenfeng, "Optimization design of nlfm signal and its pulse compression simulation," in *2005 IEEE International Radar Conference*, Jun. 2005, pp. 383–386.
- [24] T. Collins and P. Atkins, "Nonlinear frequency modulation chirps for active sonar," *IEE Proceedings-Radar, Sonar and Navigation*, vol. 146, no. 6, pp. 312–316, Dec. 1999.
- [25] K. Yue, S. Chen, and C. Shu, "Calculation of aircraft target's single-pulse detection probability," *Journal of Aerospace Technology and Management*, vol. 7, no. 3, pp. 314–322, Jul. 2015. [Online]. Available: <https://doi.org/10.5028/jatm.v7i3.470>
- [26] H. Ya-Lin, Z. Chen-Xin, L. Kai-Yue, and W. U. Sheng-Yuan, "A study on moving target detection and tracking based on radar signal," *Computer Simulation*, vol. 34, no. 89, pp. 14–17, Aug. 2017.
- [27] L. Zhanqiang, L. Lujiang, H. U. Qiyong, and W. Chunyang, "Evaluation on aircraft stealth performance based on radar detection probability," *Journal of Harbin Institute of Technology*, vol. 47, no. 11, pp. 158–166, Nov. 2017.
- [28] J. D. Wilson, "Probability of detecting aircraft targets," *IEEE Transactions on Aerospace and Electronic Systems*, vol. 8, no. 6, pp. 757–761, Nov. 1972.
- [29] G. Jian-Zhong, D. Chen-Long, and Y. Hai-Lin, "Research on the influence of the actuator dynamic characteristics on the flight characteristics of the civil aircraft," *Science Technology and Engineering*, vol. 13, no. 35, pp. 10 745–10 749, Dec. 2013.
- [30] C. Shichun, H. Peilin, and J. Jinzu, "Analysis on repeater jamming active cancellation for linear frequency modulated wave," *Journal of Beijing University of Aeronautics & Astronautics*, vol. 40, no. 7, pp. 939–946, Jul. 2014.